Mathematical Modeling of a Lithium Ion Battery

Long Cai and Ralph E. White*
Department of Chemical Engineering, University of South Carolina
*Corresponding author: 301 Main Street, Columbia, SC 29208, white@cec.sc.edu

Abstract: The existing lithium ion battery model in COMSOL's Multiphysics (MP) software is extended to include the thermal effects. The thermal behavior of a lithium ion battery is studied during the galvanostatic discharge process with and without a pulse.

Keywords: Lithium ion battery, Thermal model, Pulse discharge, Temperature

1. Introduction

The existing lithium ion battery model in COSMOL 3.5a is extended here by adding an energy balance and the temperature dependence of properties of the battery.

This thermal model is developed based on the pseudo two-dimensional (P2D) model which was described in [1, 2] and a thermal, electrochemistry coupled model. The diffusion coefficient of Li ions in the solid phase and electrolyte, the reaction rate constants of the electrochemical reactions, the open circuit potentials and the thermal conductivity of the binary electrolyte depend on the temperature in the model presented here.

2. Mathematical Model

A schematic of a lithium ion battery is shown in Figure 1.

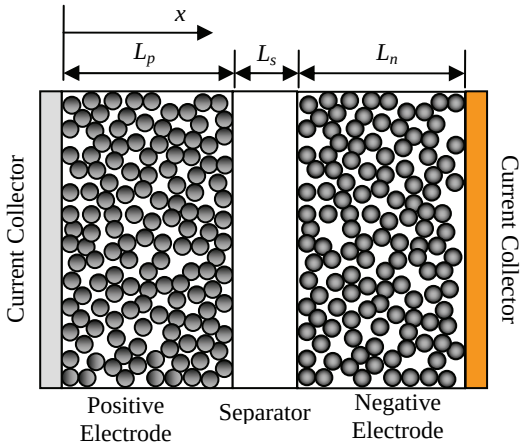

Figure 1. Schematic of a Lithium ion battery

Generally, a lithium ion battery consists of the current collector, the positive electrode, the separator and the negative electrode. A lithiated organic solution fills the porous components and serves as the electrolyte.

The material balance for the Li ions in an active solid material particle is governed by Fick's second law in spherical coordinates:

$$\frac{\partial c_{s,i}}{\partial t} = D_{s,i}\frac{1}{r^2}\frac{\partial}{\partial r}\left(r^2\frac{\partial c_{s,i}}{\partial r}\right) \qquad (1)$$

where $i=p$ for the positive electrode and $i=n$ for the negative electrode. At the center of the particle, there is no flux, that is:

$$\text{at } r=0: \; -D_{s,i}\frac{\partial c_{s,i}}{\partial r} = 0$$

On the surface of the particle, the flux is equal to the consuming/producing rate of Li ions due to the electrochemical reaction occurring at the solid/liquid interface:

$$\text{at } r=R_{s,i}: \; -D_{s,i}\frac{\partial c_{s,i}}{\partial r} = J_i$$

where J_i is the flux of lithium ions away from the surface of the spherical particles.

The material balance for the binary electrolyte in the liquid phase is given by:

$$\varepsilon_i\frac{\partial c_i}{\partial t} = D_{eff,i}\frac{\partial^2 c_i}{\partial x^2} + \left(1-t_+^0\right)a_i J_i \qquad (2)$$

where $i=p$, s, and n and a_i is the electrode surface area per unit volume of the electrode. In the separator the pore wall flux J_s is equal to zero. At the two ends of the cell in the x-direction, there is no mass flux, that is:

$$-D_{eff,p}\left.\frac{\partial c_p}{\partial x}\right|_{x=0} = 0$$

$$-D_{eff,n}\left.\frac{\partial c_n}{\partial x}\right|_{x=L_p+L_s+L_n} = 0$$

At the interfaces between the positive electrode/separator and separator/negative electrode, the concentration of the binary electrolyte and its flux are continuous

$$c_p\big|_{x=L_p^-} = c_s\big|_{x=L_p^+}$$

$$c_s\big|_{x=(L_p+L_s)^-} = c_n\big|_{x=(L_p+L_s)^+}$$

$$-D_{eff,p}\left.\frac{\partial c_p}{\partial x}\right|_{x=L_p^-} = -D_{eff,s}\left.\frac{\partial c_s}{\partial x}\right|_{x=L_p^+}$$

$$-D_{eff,s}\left.\frac{\partial c_s}{\partial x}\right|_{x=(L_p+L_s)^-} = -D_{eff,n}\left.\frac{\partial c_n}{\partial x}\right|_{x=(L_p+L_s)^+}$$

The effective diffusion coefficient of the binary electrolyte in the liquid phase is corrected by porosity [3]:

$$D_{\text{eff},i} = D_{e,i}\varepsilon_i^{\text{brugg}_i}$$

where $D_{e,i} = 10^{-4.43-\frac{54}{T-229-5.0\times10^3 c_i}-0.22\times10^3 c_i}$

The charge balance in the solid phase is governed by Ohm's law:

$$\sigma_{eff,i}\frac{\partial^2\phi_{1,i}}{\partial x^2} = a_i F J_i \qquad (3)$$

where $i=p$ and n. The effective conductivity is determined by $\sigma_{\text{eff},i} = \sigma_i\left(1-\varepsilon_i-\varepsilon_{\text{f},i}\right)$. The specific area can be calculated by $a_i = \frac{3}{R_{s,i}}\left(1-\varepsilon_i-\varepsilon_{\text{f},i}\right)$. At the interface of the current collector and the positive electrode, the charge flux is equal to the current density applied to the cell:

$$-\sigma_{eff,p}\left.\frac{\partial\phi_{1,p}}{\partial x}\right|_{x=0} = I_{\text{app}}$$

where I_{app} is the applied current density.

At the interfaces of the positive electrode/ separator and the separator/negative electrode, there is no charge flux:

$$-\sigma_{eff,p}\left.\frac{\partial\phi_{1,p}}{\partial x}\right|_{x=L_p} = 0,\ -\sigma_{eff,n}\left.\frac{\partial\phi_{1,n}}{\partial x}\right|_{x=L_p+L_s} = 0$$

The potential of the solid phase at the right end of the cell is set to zero $\left.\phi_{1,n}\right|_{x=L_p+L_s+L_n} = 0$, and the potential of the solid phase at x=0, $\left.\phi_{1,p}\right|_{x=0}$ is equal to E_{cell} (the cell voltage).

The charge balance in the liquid phase is based on Ohm's law and is given by:

$$-\frac{\partial}{\partial x}\left(\kappa_{eff,i}\frac{\partial\phi_{2,i}}{\partial x}\right) + \frac{2RT\left(1-t_+^0\right)}{F}\frac{\partial}{\partial x}\left(\kappa_{eff,i}\frac{\partial\ln c_i}{\partial x}\right) = a_i F J_i \qquad (4)$$

where $i=p$, s and n and the specific conductivity of the binary electrolyte is a function of temperature and the concentration of the binary electrolyte in the liquid phase [3]:

$$\kappa_{\text{eff},i} = \kappa_i\varepsilon_i^{\text{brugg}_i}$$

where $\kappa_i = c_i\left(\begin{array}{l}-10.5+0.668\times10^3 c_i+\\ 0.494\times10^6 c_i^2+0.074T-\\ 17.8c_iT-8.86\times10^2 c_i^2T-\\ 6.96\times10^{-5}T^2+2.80\times10^{-2}c_iT^2\end{array}\right)^2$

At the two ends of the cell, there is no charge flux in the liquid phase:

$$-\kappa_{eff,p}\left.\frac{\partial\phi_{2,p}}{\partial x}\right|_{x=0} = 0 \text{ and}$$

$$-\kappa_{eff,n}\left.\frac{\partial\phi_{2,n}}{\partial x}\right|_{x=L_p+L_s+L_n} = 0$$

The potential in the solution phase and its flux are continuous at the interfaces of the electrodes and the separator.

In the above equations the pore wall flux, J_i, is determined by the Bulter-Volmer equation:

$$J_i = k_i\left(c_{s,i,\max}-c_{s,i,\text{surf}}\right)^{0.5}c_{s,i,\text{surf}}^{0.5}c_i^{0.5}\left[\exp\left(\frac{0.5F}{RT}\eta_i\right)-\exp\left(-\frac{0.5F}{RT}\eta_i\right)\right] \qquad (5)$$

and the over potential of the intercalation reaction is given by:

$$\eta_i = \phi_{1,i}-\phi_{2,i}-U_i$$

The energy balance is given by [4, 5]:

$$\rho C_p\frac{dT}{dt} = \lambda\frac{\partial^2T}{\partial x^2}+Q_{\text{rxn}}+Q_{\text{rev}}+Q_{\text{ohm}} \qquad (6)$$

with the boundary conditions determined by Newton's cooling law:

$$-\lambda\left.\frac{\partial T}{\partial x}\right|_{x=0} = h\left(T_\infty-T\right)$$

$$-\lambda\left.\frac{\partial T}{\partial x}\right|_{x=L_p+L_s+L_n} = h\left(T-T_\infty\right)$$

where h is the heat transfer coefficient, T_∞ is the environmental temperature, Q_{rxn} is the total reaction heat generation rate, Q_{rev} is the total reversible heat generation rate, Q_{ohm} is the total ohmic heat generation rate. The heat fluxes are defined by:

$$Q_{\text{rxn}} = FaJ\left(\phi_1-\phi_2-U\right)$$

$$Q_{\text{rev}} = FaJT\frac{\partial U}{\partial T}$$

$$Q_{\text{ohm}} = \sigma_{\text{eff}} \left(\frac{\partial \phi_1}{\partial x} \right)^2 + \kappa_{\text{eff}} \left(\frac{\partial \phi_2}{\partial x} \right)^2 + \frac{2\kappa_{\text{eff}} RT}{F} \left(1 - t_+^0\right) \frac{1}{c} \frac{\partial c}{\partial x} \frac{\partial \phi_2}{\partial x}$$

The temperature dependent open circuit potential of electrode i is approximated by Taylor's first order expansion around a reference temperature:

$$U_i = U_{i,\text{ref}} + \left(T - T_{\text{ref}}\right) \left[\frac{dU}{dT} \right]_i$$

where $U_{i,\text{ref}}$ is the open circuit potential under the reference temperature T_{ref}.

3. COMSOL Model

The mathematical model described in section 2 is a multi-scale model. We developed several geometries in COMSOL: a 1D geometry which consists of three sequentially connected lines to represent the positive electrode, the separator and the negative electrode, respectively, a 2D geometry which consists of two rectangles to denote the solid phase in the electrodes. The geometries are shown in Figure 2. The vertical coordinate in the 2D geometry indicates the radial direction of the solid particles. Since we ignore the diffusion of Li ions in the x-direction in the particle, the corresponding diffusion coefficient is set to zero in this direction. The concentration of the binary electrolyte, the potential in the electrolyte, the potential in the solid phase and the pore wall flux are solved in the 1D geometry. The concentration of Li ions in the solid phase is solved in the 2D geometry. The pore wall flux is extruded from the 1D domain and projected to the top boundary of the 2D geometry by using "subdomain extrusion coupling variables" in COMSOL. The concentration of Li ions on the top boundary in the 2D geometry is projected to the 1D domain by using "boundary extrusion coupling variables".

The thermal behavior of the Li ion battery during pulse discharge is also simulated in COSMOL. The battery is discharged for 3000s at C/2 rate first and then discharged at 3C rate until the cell voltage drops to 2.5V. The change of the applied current density is implemented by using the smoothed Heaviside function "flsmhs" and is shown in Figure 3.

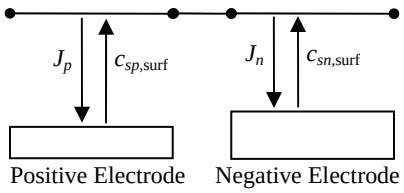

Figure 2. Geometries and variables coupling between the geometries in COSMOL (The top 1D geometry consists of three segments which denote the positive electrode, the separator and the negative electrode. The bottum two rectangles represent the solid phases in the positive electrode and the negative electrode, respectively. The pore wall flux is extracted from the 1D geometry and projected to the top boundary of the 2D geometry. The concentration of Li ions on the top boundary of the 2D geometry is projected to the 1D domain as the surface concentration of the solid particles.)

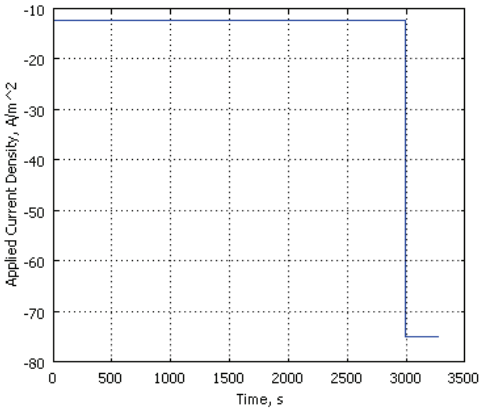

Figure 3. Current density profile in the discharge process including a 3C pulse

4. Simulation Results

Figure 4 shows the temperature on the cell surface at 1C discharge process under three different cooling conditions where the heat transfer coefficient is 10.0, 1.0 and 0.1 W/m^2/K, respectively, and two limiting conditions: the isothermal condition and the adiabatic condition.

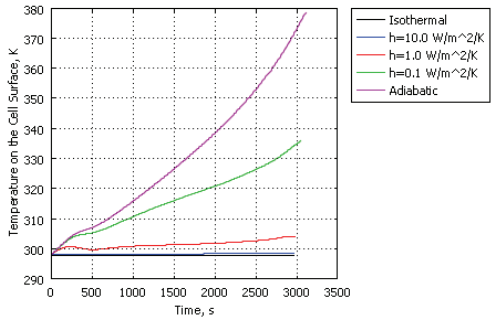

Figure 4. Temperature on the cell surface during 1C discharge process under different cooling conditions

The thermal effect on the cell voltage is shown in Fiugre 5. The cell provides more discharge capacity when it is placed in a better heat isolation environment (i.e. adiabatic condition). In a better isolated environment, the cell temperautre increases faster during the 1C discharge process which results in the higher diffusion coefficient for the binary electrolyte and reduces the diffusion limitations.

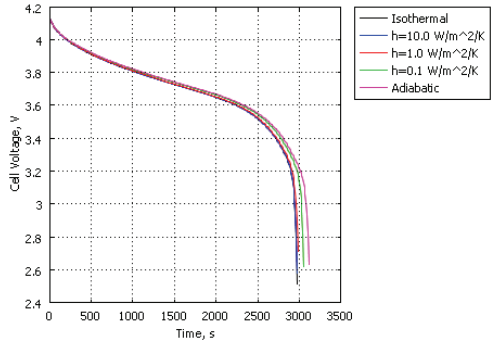

Figure 5. Cell Voltage for 1C discharge process under different cooling conditions

The reduction of the diffusion limit in the binary electrolyte can be verified by comparing the concentration profile of the electrolyte under different cooling conditions. Figure 6 shows the concentration profiles of the electrolyte at the end of 1C discharge process under the two limiting conditions. The concentration profile under the adiabatic condition is flatter than that in the isothermal case, which indicates a better diffusion property in the electrolyte under the adiabatic condition than under the isothermal condition.

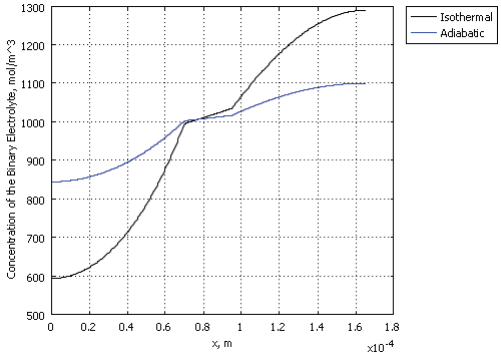

Figure 6. Comparison of the concentration profiles of the binary electrolyte at the end of the 1C discharge process under the isothermal condition and the adiabatic condition

Figure 7 shows the cell temperature during the 1C discharge process at different current rates as the heat transfer coefficient is 1.0 W/m^2/K. As expected, the cell gets hotter as the dishcarge current rate increases. It is also noticed that the wave part which appears in beginning of the temperature curve at low current rate (less than 2C) does not exist in the high current rate cases. The wave part on the temperature curve is characterised by the reversible heat generation during discharging. Under low current rate discharging, the reversible heat is roughly equivelant to the ohmic heat, but becomes unimportant as the discharge current rate increases.

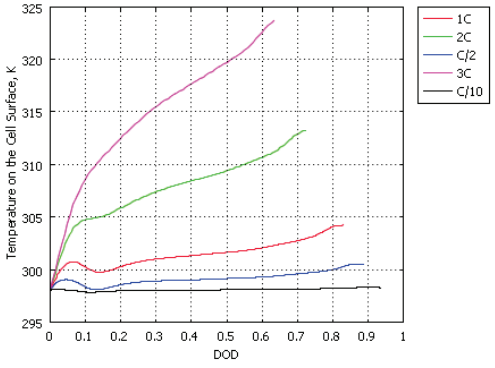

Figure 7. Temperature on the cell surface during discharge process under different current rates while the heat transfer coefficient h=1.0 W/m^2/K where the DOD is defined as: DOD=time * C rate / 3600

The P2D model mentioned in section 2 is also useful for simulating the discharge process with pulse. Figure 8 shows the cell voltage during the C/2 discharge for 3000s followed by a 3C pulse discharge until the cell voltage drops to 2.5V. The corresponding temperature on the surface of the cell is also plotted in Figure 9. The surface temperature at the end of the 3C pulse is slightly less than that in the pure 3C discharge process.

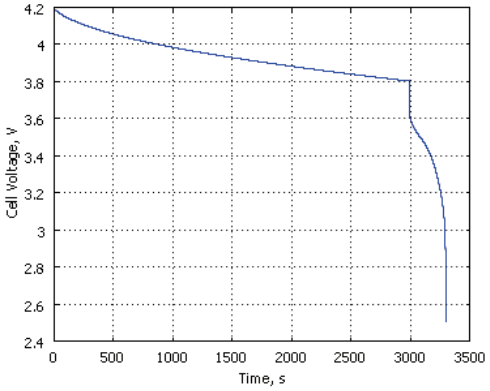

Figure 8. Cell Voltage at C/2 discharge for 3000s followed by a 3C pulse discharge

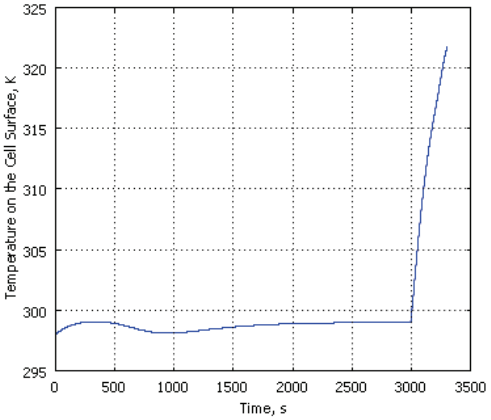

Figure 9. Temperature on the cell surface in the discharge process with 3C pulse

Figure 10 shows the concentration of the binary electrolyte at the two ends of the cell during the pulse discharge process. At the beginning of the pulse, the concentration of the electrolyte changes extremely, after that it relaxes and tend to a stable value.

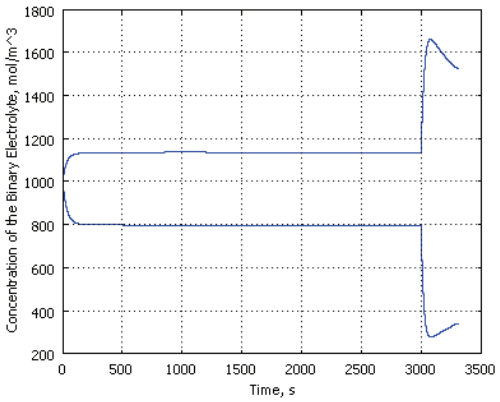

Figure 10. Concentration of the binary electrolyte at the two ends of the cell (the bottom line is at x=0, the top line is at x=1.65e-4) in the C/2 discharge process with a 3C pulse

5. Conclusions

The thermal behavior of a Lithium ion battery during galvanostatic discharge w/o pulse can be predicted by using COMSOL Multiphysics. Though better thermal isolation environment improves the discharge capacity, the higher cell temperature raises the risk of thermal runaway and more rapid wear out of the cell.

6. References

1. M. Doyle, T.F. Fuller and J. Newman, Modeling of galvanostatic charge and discharge of the Lithium/Polymer/Insertion cell, *Journal of Electrochemical Society*, **140**, 1526-1533 (1993)

2. T.F. Fuller, M. Doyle, and J. Newman, Simulation and Optimization of the Dual Lithium Ion Insertion Cell, *Journal of Electrochemical Society*, **141**, 1-10 (1994)

3. Lars Ole Valoen, and N. Reimers, Transport Properties of $LiPF_6$-Based Li-Ion Battery Electrolytes, *JES*, **152**, A882-A891 (2005)

4. W.B. Gu and C.Y. Wang, Thermal-Electrochemical Modeling of Battery System, *Journal of Electrochemical Society*, **147**, 2910-2922 (2000)

5. K. Kumaresan, G. Sikha and R.E. White, *Thermal Model for a Li-Ion Cell. Journal of the Electrochemical Society*, **155**, A164-A171 (2008)